

High-sensitivity phase estimation with a two-mode squeezed coherent state based on a Mach-Zehnder interferometer

Pengxiang Ruan(阮鹏祥), Jun Liu(刘俊), Chenlu Li(李晨露), Qingli Jing(荆庆丽), Mingming Zhang(张明明), and Dong-Xu Chen(陈东旭)

Citation: Chin. Phys. B, 2026, 35 (**2**): 024203. DOI: 10.1088/1674-1056/adf4ad
http://cpb.iphy.ac.cn; http://iopscience.iop.org/cpb

What follows is a list of articles you may be interested in

Quantum optical interferometry via general photon-subtracted two-mode squeezed states

Li-Li Hou(侯丽丽), Jian-Zhong Xue(薛建忠), Yong-Xing Sui(眭永兴), Shuai Wang(王帅)
Chin. Phys. B, 2019, 28 (**9**): 094217. DOI: 10.1088/1674-1056/ab38a9

Super-sensitive phase estimation with coherent boosted light using parity measurements

Lan Xu(许兰), Qing-Shou Tan(谭庆收)
Chin. Phys. B, 2018, 27 (**1**): 014203. DOI: 10.1088/1674-1056/27/1/014203

Phase estimation of phase shifts in two arms for an SU(1,1) interferometer with coherent and squeezed vacuum states

Qian-Kun Gong(龚乾坤), Dong Li(李栋), Chun-Hua Yuan(袁春华), Ze-Yu Qu(区泽宇), Wei-Ping Zhang(张卫平)
Chin. Phys. B, 2017, 26 (**9**): 094205. DOI: 10.1088/1674-1056/26/9/094205

Super-resolution and super-sensitivity of entangled squeezed vacuum state using optimal detection strategy

Jiandong Zhang(张建东), Zijing Zhang(张子静), Longzhu Cen(岑龙柱), Shuo Li(李硕), Yuan Zhao(赵远), Feng Wang(王峰)
Chin. Phys. B, 2017, 26 (**9**): 094204. DOI: 10.1088/1674-1056/26/9/094204

Photon statistical properties of photon-added two-mode squeezed coherent states

Xu Xue-Fen (许雪芬), Wang Shuai (王帅), Tang Bin (唐斌)
Chin. Phys. B, 2014, 23 (**2**): 024206. DOI: 10.1088/1674-1056/23/2/024206

High-sensitivity phase estimation with a two-mode squeezed coherent state based on a Mach–Zehnder interferometer

Pengxiang Ruan(阮鹏祥)[1], Jun Liu(刘俊)[1,†], Chenlu Li(李晨露)[1], Qingli Jing(荆庆丽)[1], Mingming Zhang(张明明)[1], and Dong-Xu Chen(陈东旭)[2,‡]

[1] *School of Science, Jiangsu University of Science and Technology, Zhenjiang* 212003, *China*
[2] *Quantum Information Research Center, Shangrao Normal University, Shangrao* 334001, *China*

(Received 21 May 2025; revised manuscript received 18 July 2025; accepted manuscript online 28 July 2025)

A scheme is proposed based on a Mach–Zehnder interferometer with high phase sensitivity, utilizing a two-mode squeezed coherent state, generated by four-wave mixing, as input. The phase sensitivity of this scheme easily surpasses the Heisenberg limit when intensity difference detection is applied. Under phase-matching conditions, the quantum Cramér–Rao bound significantly exceeds the Heisenberg limit. Additionally, the scheme exhibits robustness against photon loss. When compared with the modified SU(1,1) interferometer with two coherent state inputs, this approach demonstrates superior measurement sensitivity, evaluated through various detection methods and the quantum Cramér–Rao bound. This work holds potential applications in quantum metrology.

Keywords: two-mode squeezed coherent state, phase estimation, quantum Cramér–Rao bound, Heisenberg limit

PACS: 42.50.–p, 03.65.Ta, 42.50.St

DOI: 10.1088/1674-1056/adf4ad **CSTR:** 32038.14.CPB.adf4ad

1. Introduction

The widely studied Mach–Zehnder interferometer (MZI) is one of the most crucial optical interferometers in quantum information.[1–3] It is commonly used to estimate tiny phase shifts in quantum precision measurements.[4–9] Zuo *et al.* experimentally demonstrated that employing an MZI enables the measurement of detectable phase shifts surpassing the shot-noise limit (SNL).[10] An MZI consists of two beam splitters (BSs) and two paths of equal length. When the input to an MZI is two coherent beams, the measurement sensitivity is limited by the SNL.[11]

Many research groups have achieved higher precision by introducing various input states, such as two-mode squeezed vacuum states,[11,12] NOON states,[13] twin Fock states and so on.[14–19] With these modifications, the phase sensitivity of the MZI can surpass the SNL and even reach the Heisenberg limit (HL). In this context, beating the HL has become a pressing issue for researchers. Numerous attempts and diverse approaches have been explored to achieve this goal.[15,20–23] It has been predicted that the phase sensitivity of an MZI could reach the HL with the input of a single-mode squeezed vacuum beam.[21,24,25] Moreover, efforts have been made to enhance the degree of squeezing of the input states for higher precision.[9,26–30]

On the other hand, surpassing the HL can also be achieved by adopting different detection methods, such as balanced homodyne detection,[31] parity detection,[9] intensity difference detection (IDD)[32,33] and intensity sum detection.[34] However, in practical experiments, it is impossible to implement all measurement methods simultaneously. To address this issue, Braunstein and Caves introduced the quantum Cramér–Rao bound (QCRB).[35] The QCRB provides the optimal theoretical limit without relying on specific measurement strategies, effectively solving the problem of experimentally exhausting all possible detection methods. Therefore, in the field of precision measurement, the QCRB is frequently used to evaluate the performance of different schemes.

In recent times, numerous precision measurement works based on an MZI have been published. These studies employed various input states and achieved notable phase sensitivity with different detection methods, as well as with respect to the QCRB.[36] For example, Zhang *et al.* selected a multi-photon catalysis two-mode squeezed vacuum state as the input state, which improved the phase sensitivity.[9] Ataman *et al.* chose two coherent light beams as the input state, and used two different detection methods to reach the QCRB.[37] Liu *et al.* employed a squeezed coherent light beam along with vacuum light in their scheme, achieving phase sensitivity that beats the SNL.[38] Zhang *et al.* applied a number-conserving generalized superposition of product operations on a two-mode squeezed vacuum state as the input to the MZI to obtain phase sensitivity that can consistently surpass the SNL.[39] Haldar *et al.* employed a two-mode squeezed coherent state as the input

†Corresponding author. E-mail: junliu@just.edu.cn
‡Corresponding author. E-mail: chendx@sru.edu.cn

© 2026 Chinese Physical Society and IOP Publishing Ltd. All rights, including for text and data mining, AI training, and similar technologies, are reserved.

and introduced losses in both arms of an MZI to investigate internal losses. Their work provided an in-depth analysis in this area.[23] In contrast to previous studies, our research focuses more on the ultimate precision achievable with the two-mode squeezed coherent state and the conditions required to reach such high precision. To this end, we introduce the QCRB, SNL and HL as benchmarks, which allows us to explore the problem from multiple perspectives. Moreover, while studying losses we concentrate on external losses at the detection stage, thus addressing a gap that has been less explored in earlier research.

In this paper, we utilize a two-mode squeezed coherent state as the input to the MZI and investigate the phase-matching relation by studying the phase of the input light. Liu *et al.* experimentally implemented the relation.[40] This relation helps identify the point of phase sensitivity that can surpass the SNL and the HL. We calculate the QCRB to evaluate the ultimate accuracy of our scheme by studying multiple parameter combinations. On the other hand, photon loss is inevitable in practical applications. Therefore, we also study the effect of photon loss on phase sensitivity by placing fictitious beam splitters (FBSs) in front of the detectors to simulate photon loss. Additionally, we compare our scheme with existing ones, such as a phase-insensitive modified SU(1,1) interferometer based on two coherent-state inputs.[41] Our scheme exhibits superior phase sensitivity at low photon numbers.

This paper is arranged as follows. In Section 2, we begin by presenting the fundamental structure of the MZI and its input–output relationship. Then, we consider the input state to be a two-mode squeezed coherent state generated by four-wave mixing (FWM) and derive the corresponding output state. The phase sensitivity is evaluated by the intensity-difference detection method. In Section 3, we compare the phase sensitivity, the QCRB, the SNL and the HL. We investigate the dependence of phase sensitivity on different experimental parameters and establish the phase-matching relationship. We also analyze the system's tolerance to photon loss. In Section 4, we compare our scheme with existing ones. Finally, in Section 5, we summarize our work.

2. Measurement sensitivities of an MZI

In this section, as the foundation of our measurement scheme, we first introduce the configuration of an MZI with two coherent states. Then, we describe our MZI scheme based on a two-mode squeezed coherent state generated by FWM.

2.1. MZI with two coherent states

A schematic of an MZI with two coherent states is shown in Fig. 1, where two coherent modes interact at the first 50:50 BS without passing through the FWM section indicated by the first dashed part. Two phase shifters are placed in the two arms of the interferometer. After the phase shifts ϕ_1 and ϕ_2, the two beams are combined at the second 50:50 BS and are finally detected by the detectors for intensity measurement.

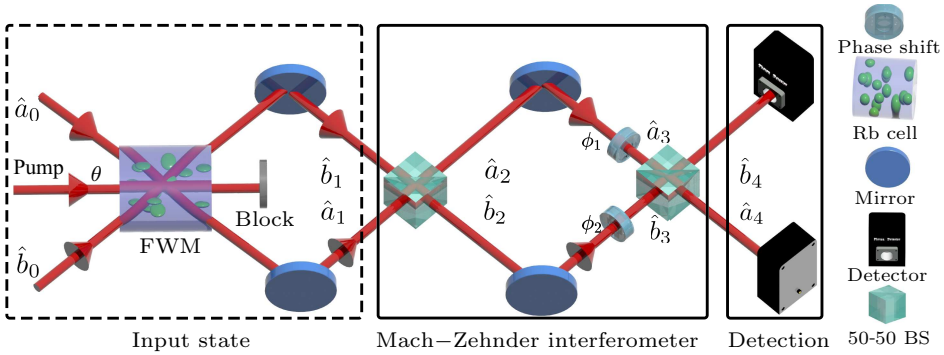


Fig. 1. Two coherent beams pass through a Rb cell to produce a two-mode squeezed coherent state that serves as the input of the MZI. The output states of the MZI are then subjected to intensity difference detection by the detectors. θ is the total phase shift of the FWM. ϕ_1 and ϕ_2 are the phase shifts of the phase shifters. We set $\phi_1 = \phi$ and $\phi_2 = 0$. FWM, four-wave mixing; BS, 50:50 beam splitter.

The relation between the output and input modes of the first 50:50 BS is given by

$$\hat{a}_2 = \frac{1}{\sqrt{2}}\hat{a}_1 + \mathrm{i}\frac{1}{\sqrt{2}}\hat{b}_1, \tag{1}$$

$$\hat{b}_2 = \mathrm{i}\frac{1}{\sqrt{2}}\hat{a}_1 + \frac{1}{\sqrt{2}}\hat{b}_1, \tag{2}$$

where $\hat{a}_1$ and $\hat{b}_1$ represent the two input modes and the light intensities are $I_{a_1} = \langle \hat{a}_1^\dagger \hat{a}_1 \rangle$ and $I_{b_1} = \langle \hat{b}_1^\dagger \hat{b}_1 \rangle$. In this part, we set the phase $\phi_1 = \phi$, $\phi_2 = 0$. We focus on the phase difference between the two arms.

Subsequently, the two beams go through the phase shifters: $\hat{a}_3 = \hat{a}_2 \mathrm{e}^{\mathrm{i}\phi}$, $\hat{b}_3 = \hat{b}_2$. Then they combine on the second BS; the output modes are

$$\hat{a}_4 = \frac{1}{\sqrt{2}}\hat{a}_3 + \mathrm{i}\frac{1}{\sqrt{2}}\hat{b}_3 = \frac{\hat{a}_1}{2}(\mathrm{e}^{\mathrm{i}\phi} - 1) + \mathrm{i}\frac{\hat{b}_1}{2}(\mathrm{e}^{\mathrm{i}\phi} + 1), \tag{3}$$

$$\hat{b}_4 = \mathrm{i}\frac{1}{\sqrt{2}}\hat{a}_3 + \frac{1}{\sqrt{2}}\hat{b}_3 = \mathrm{i}\frac{\hat{a}_1}{2}(\mathrm{e}^{\mathrm{i}\phi} + 1) + \frac{\hat{b}_1}{2}(1 - \mathrm{e}^{\mathrm{i}\phi}). \tag{4}$$

According to Eqs. (3) and (4), the intensities of the two output modes from the second BS of the interferometer are

respectively given by

$$\begin{aligned}\langle \hat{I}_{a_4}\rangle &= \langle \hat{a}_4^\dagger \hat{a}_4\rangle \\ &= \frac{1-\cos\phi}{2}\langle \hat{a}_1^\dagger \hat{a}_1\rangle + \frac{\sin\phi}{2}\langle \hat{a}_1^\dagger \hat{b}_1\rangle \\ &\quad + \frac{\sin\phi}{2}\langle \hat{b}_1^\dagger \hat{a}_1\rangle + \frac{1+\cos\phi}{2}\langle \hat{b}_1^\dagger \hat{b}_1\rangle, \qquad (5)\\ \langle \hat{I}_{b_4}\rangle &= \langle \hat{b}_4^\dagger \hat{b}_4\rangle \\ &= \frac{1+\cos\phi}{2}\langle \hat{a}_1^\dagger \hat{a}_1\rangle - \frac{\sin\phi}{2}\langle \hat{a}_1^\dagger \hat{b}_1\rangle \\ &\quad - \frac{\sin\phi}{2}\langle \hat{b}_1^\dagger \hat{a}_1\rangle + \frac{1-\cos\phi}{2}\langle \hat{b}_1^\dagger \hat{b}_1\rangle, \qquad (6)\end{aligned}$$

where $\hat{a}_i$, $\hat{b}_i$, $\hat{a}_i^\dagger$ and $\hat{b}_i^\dagger$ ($i = 2, 3, 4$) are annihilation and creation operators of the modes during the process.

2.2. MZI with a two-mode squeezed coherent state

Next, we consider a two-mode squeezed coherent state as the input of the MZI; this is generated by the FWM in the dashed box in Fig. 1. The generated two-mode squeezed state then passes through the MZI.

The relation between the output and input modes of the FWM process is given by[38,42]

$$\hat{a}_1 = \cosh r\hat{a}_0 + \mathrm{e}^{\mathrm{i}\theta}\sinh r\hat{b}_0^\dagger, \qquad (7)$$

$$\hat{b}_1 = \mathrm{e}^{\mathrm{i}\theta}\sinh r\hat{a}_0^\dagger + \cosh r\hat{b}_0, \qquad (8)$$

where r is the parametric strength and θ is the total phase shift of the FWM. $\hat{a}_0$, $\hat{b}_0$, $\hat{a}_0^\dagger$ and $\hat{b}_0^\dagger$ are annihilation and creation operators of the input probe modes. For the coherent input beam, we have $\langle \hat{a}_0\rangle = \mathrm{e}^{\mathrm{i}\theta_a}|\alpha_a|$, $\langle \hat{b}_0\rangle = \mathrm{e}^{\mathrm{i}\theta_b}|\alpha_b|$, $\langle \hat{a}_0^\dagger\rangle = \mathrm{e}^{-\mathrm{i}\theta_a}|\alpha_a|$, $\langle \hat{b}_0^\dagger\rangle = \mathrm{e}^{-\mathrm{i}\theta_b}|\alpha_b|$, $N_a = |\alpha_a|^2$ and $N_b = |\alpha_b|^2$, where N_a, N_b, θ_a and θ_b represent the photon numbers and phases of the input light, respectively. After the FWM process, the total photon number of the amplified probe beams is

$$\begin{aligned}N &= I_{a_1} + I_{b_1} \\ &= (\cosh^2 r + \sinh^2 r)(N_a + N_b) + 2\sinh^2 r \\ &\quad + 4\cosh r\sinh r\sqrt{N_a N_b}\cos(\theta - \theta_a - \theta_b). \qquad (9)\end{aligned}$$

The input state must satisfy the condition $N \geq 1$. The SNL and HL are $1/\sqrt{N}$ and $1/N$,[12] respectively. The output intensity of the interferometer can be obtained by simultaneously solving Eqs. (5)–(8). To achieve the optimal phase sensitivity, we introduce the QCRB (see Appendix A for details),[43–48] which is given by

$$(\Delta\phi_{\mathrm{d}})^2 \geq \frac{1}{F}, \quad F = \frac{F_{\mathrm{dd}}F_{\mathrm{ss}} - F_{\mathrm{ds}}F_{\mathrm{sd}}}{F_{\mathrm{ss}}}, \qquad (10)$$

where F_{dd}, F_{ds}, F_{sd} and F_{ss} are the difference–difference, difference–sum, sum–difference and sum–sum Fisher matrix elements of F, which are given by

$$\begin{aligned}F_{\mathrm{dd}} &= F_{\mathrm{ss}} \\ &= [(1 + 8\sinh^2 r + 8\sinh^4 r)](N_a + N_b) \\ &\quad + 8[\cosh^3 r\sinh r + \cosh r\sinh^3 r] \\ &\quad \times\sqrt{N_a N_b}\cos(\theta - \theta_a - \theta_b) + 4[\sinh^2 r + \sinh^4 r], \\ F_{\mathrm{ds}} &= F_{\mathrm{sd}} \\ &= 4N_a[\cosh^3 r\sinh r + \cosh r\sinh^3 r]\sin(\theta - 2\theta_a) \\ &\quad - 4N_b[\cosh^3 r\sinh r + \cosh r\sinh^3 r]\sin(\theta - 2\theta_b) \\ &\quad - 2\sqrt{N_a N_b}[\cosh^4 r + 6\cosh^2 r\sinh^2 r \\ &\quad + \sinh^4 r]\sin(\theta_a - \theta_b). \qquad (11)\end{aligned}$$

As indicated by Eq. (11), $\Delta\phi_{\mathrm{d}}$ decreases as F increases. By substituting Eq. (11) into Eq. (10), we find that to minimize $\Delta\phi_{\mathrm{d}}$ we need to maximize F. Since F_{dd} and F_{ds} are larger than 0, to maximize F we need to maximize F_{dd} and minimize F_{ds}. Achieving the maximum value of F requires $\theta - \theta_a - \theta_b = 2k\pi$, $\theta - 2\theta_a = k\pi$, $\theta - 2\theta_b = k\pi$ and $\theta_a - \theta_b = k\pi$, where k is an integer. In this case, the QCRB can be written as

$$\Delta\phi_{\mathrm{QCRB}} = (\Delta\phi_{\mathrm{d}})_{\min} = \frac{1}{\sqrt{F_{\mathrm{dd}}}}. \qquad (12)$$

2.3. Intensity difference detection

In this work, we employ the intensity difference detection method to obtain the phase sensitivity. The intensity difference of the output of the MZI is given by

$$\hat{I}_- = \hat{a}_4^\dagger \hat{a}_4 - \hat{b}_4^\dagger \hat{b}_4. \qquad (13)$$

The observable $\hat{I}_-$ depends on the parameter ϕ, which is the phase shift in the MZI. The expectation value of $\hat{I}_-$ is $\langle \hat{I}_-(\phi)\rangle = \langle \psi_{\mathrm{in}}|\hat{I}_-(\phi)|\psi_{\mathrm{in}}\rangle$, which is

$$\langle \hat{I}_-\rangle = \langle \psi_{\mathrm{in}}|\hat{a}_4^\dagger \hat{a}_4 - \hat{b}_4^\dagger \hat{b}_4|\psi_{\mathrm{in}}\rangle. \qquad (14)$$

The phase sensitivity is given by

$$\Delta\phi = \frac{\Delta\hat{I}_-}{|\frac{\partial}{\partial\phi}\langle \hat{I}_-\rangle|}, \qquad (15)$$

where $\Delta\hat{I}_- = [\langle \hat{I}_-^2\rangle - \langle \hat{I}_-\rangle^2]^{1/2}$ is the standard deviation of $\hat{I}_-$. To evaluate $\Delta\phi$, we need to calculate the numerator and the denominator in Eq. (15). First, the square of the numerator is given by

$$\begin{aligned}\Delta^2\hat{I}_- &= \langle \hat{I}_-^2\rangle - \langle \hat{I}_-\rangle^2 \\ &= (N_a + N_b) + 4\sin^2\phi(\cosh^4 r - \cosh^2 r) \\ &\quad \times(2N_a + 2N_b + 1) \\ &\quad + 2\sin(2\phi)\cosh r\sinh r[N_b\cos(\theta - 2\theta_b) \\ &\quad - N_a\cos(\theta - 2\theta_a)] \\ &\quad + 8\sin^2\phi\cosh r\sinh r(\cosh^2 r + \sinh^2 r) \\ &\quad \times\sqrt{N_a N_b}\cos(\theta - \theta_a - \theta_b). \qquad (16)\end{aligned}$$

To estimate the phase sensitivity in Eq. (15), we need the absolute value of the derivative

$$\left|\frac{\partial}{\partial\phi}\langle \hat{I}_-\rangle\right| = |\sin\phi(N_a - N_b)$$

$$+2\cos\phi\cosh r\sinh r[\cos(\theta-2\theta_a)+\cos(\theta-2\theta_b)]+2\cos\phi(\cosh^2 r+\sinh^2 r)\sqrt{N_aN_b}\times\cos(\theta_a-\theta_b)|. \quad (17)$$

Therefore, for a specific two-mode squeezed coherent input state we can calculate the phase sensitivity based on Eqs. (16) and (17). The detailed results are elaborated in the next section.

3. Discussion on phase sensitivity

The quantum Fisher information associated with the well-known QCRB has been widely used to study phase sensitivity in quantum metrology.[43] In this section, we discuss the various factors that can improve phase sensitivity.

3.1. Phase sensitivity versus different input parameters

We need to optimize the six parameters in Eq. (15), which define the two-mode squeezed coherent state, to find the optimal phase point. In the following, as shown in Fig. 2, we analyze the effects of these six parameters on the phase sensitivity.

In Fig. 2(a), we optimize the six parameters (N_a, N_b, r, θ, θ_a and θ_b) to obtain the point of phase sensitivity by IDD, which can beat the SNL and the HL. When $N_a = N_b = 0.3$, $r = 0.256$ and $\theta = \theta_a = \theta_b = \pi/10$, the minimum point of phase sensitivity by IDD can easily surpass the SNL. At this point $N \geq 1$, satisfying the condition of our scheme. Additionally, the QCRB is significantly lower than both the SNL and the HL.

In Fig. 2(b), we investigate the effect of N_a on the phase sensitivity. r, θ, θ_a, θ_b and N_b take the same values as those in Fig. 2(a). For each N_a, we vary ϕ and find the minimum of the phase sensitivity by IDD. It is observed that as N_a increases all four quantities decrease. At the intersection point of the SNL and the HL, $N_a = 0.24$. The total photon number of the input modes, expressed in Eq. (9), is $N = 1$.

In Fig. 2(c), we show the phase sensitivity versus the parametric strength r. Apart from the blue line representing the SNL, the other lines eventually converge. However, it is important to note that the phase sensitivity is lower than the HL when $r < 0.43$. When $r < 0.81$, the QCRB is lower than the HL.

Finally, the effect of θ is studied in Fig. 2(d). As θ varies between 0 and 2π, the sensitivity fluctuates and becomes the minimum at $\theta = \pi/4$.

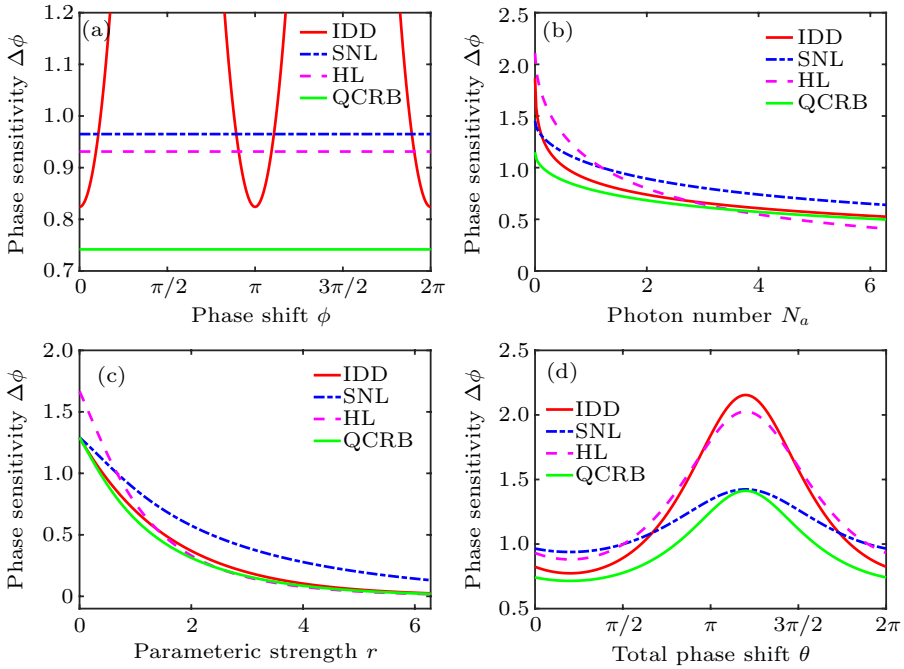


Fig. 2. Phase sensitivity versus phase shift ϕ (a), photon number N_a (b), parametric strength r (c) and total phase shift of the FWM θ (d). In (a), $N_a = N_b = 0.3$, $r = 0.256$ and $\theta = \theta_a = \theta_b = \pi/10$. In (b)–(d), other parameters are set the same as those in (a). IDD, intensity difference detection; SNL, shot noise limit; HL, Heisenberg limit; QCRB, quantum Cramér–Rao bound.

The phase sensitivity of the interferometer increases with the increase of the photon number. As shown in Fig. 3, when the photon number is sufficiently large the scheme does not surpass the HL; instead, the phase sensitivity lies between the SNL and the HL. We further investigate the effect of photon numbers N_a and N_b on the phase sensitivity in Fig. 4. As N_a and N_b increase, the phase sensitivity improves. Meanwhile, the phase sensitivity is symmetrically distributed with respect to N_a and N_b, which means that photon numbers N_a and N_b have an equal influence on the phase sensitivity.

Next, we study the phase-matching condition between θ_a and θ_b in Fig. 5. We introduce the relative HL detection

sensitivity (RHLDS), which is the difference between the HL and the phase sensitivity. A positive RHLDS means that the phase sensitivity surpasses the HL. In Fig. 5, the red, purple and blue lines represent the optimal phase points. We can see that at the optimal phase points θ_a and θ_a satisfy the relation $\theta_a - \theta_b = k\pi$, where k is an integer. Such a phase-matching condition was verified in Eq. (14).

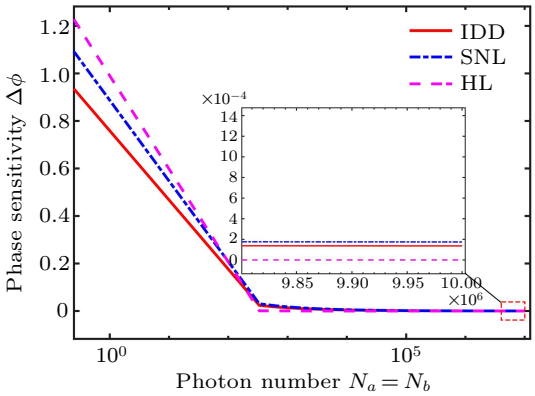


Fig. 3. Phase sensitivity versus photon numbers N_a and N_b with $r = 0.256$ and $\theta = 2\theta_a = 2\theta_b = \pi/10$.

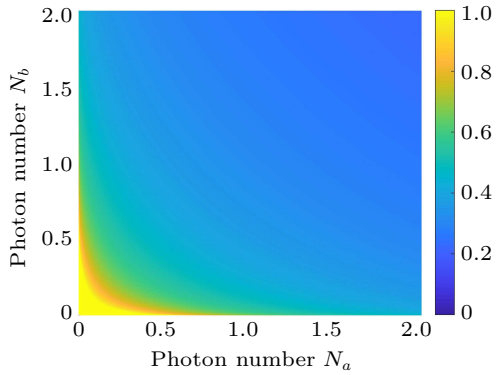


Fig. 4. Phase sensitivity versus photon numbers N_a and N_b with $r = 0.4$ and $\theta = 2\theta_a = 2\theta_b = \pi/5$.

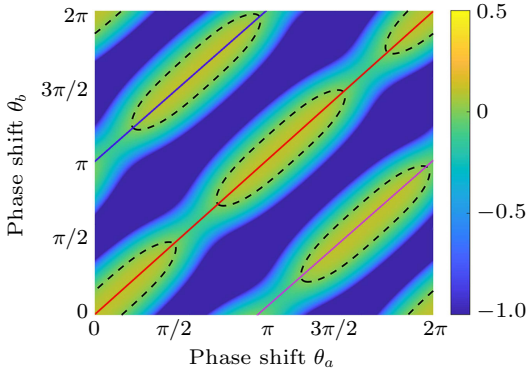


Fig. 5. Dependence of relative HL detection sensitivity (RHLDS) on θ_a and θ_b. A positive RHLDS means that the phase sensitivity surpasses the HL. $N_a = N_b = 3$ and $\theta = \pi/5$. The red line represents $\theta_a = \theta_b$, the purple line represents $\theta_a = \theta_b + \pi$ and the blue line represents $\theta_a = \theta_b - \pi$.

We further examine the effects of the parametric strength r and the total phase shift θ on RHLDS to facilitate identifying the optimal phase point. As shown in Fig. 6, the black line represents the points where RHLDS is equal to zero. We can see from Fig. 6 that when the total phase shift θ is small, the RHLDS is greater than 0 for r between 0 and 2.

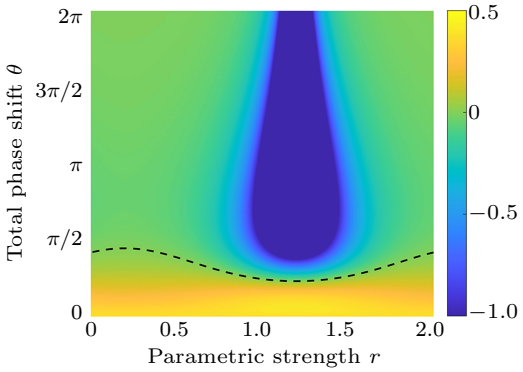


Fig. 6. Relative Heisenberg limit detection sensitivity versus parametric strength r and total phase shift θ. $N_a = N_b = 0.3$ and $\theta_a = \theta_b = \pi/10$. The black dashed line represents the case when the phase sensitivity equals the HL. The regions above zero indicate superior phase sensitivity.

3.2. Effect of photon loss on phase sensitivity

Photon loss occurs during the detection process due to the nonideal efficiency of the detectors. In the following, we use FBSs to simulate photon loss.[32] The detection inefficiency can be equivalently modeled as the transmissivity of the FBSs placed before the detectors. Therefore, detector inefficiency can be incorporated into the error propagation formula.

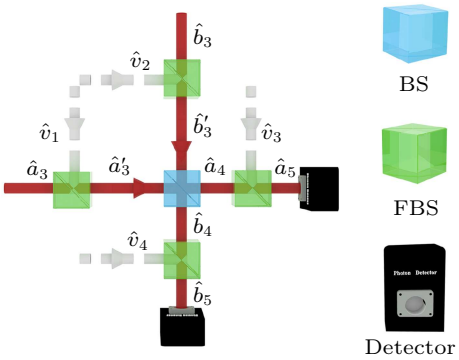


Fig. 7. Two fictitious beam splitters (FBSs) are placed before the detectors to simulate photon loss. $\hat{v}_1$, $\hat{v}_2$, $\hat{v}_3$ and $\hat{v}_4$ represent two vacuum beams. BS, beam splitter.

As shown in Fig. 7, we add two FBSs in front of the detectors to simulate detection loss. These FBSs have transmissivities denoted by T_1, T_2, T_3 and T_4, respectively. The output of the FBSs can be expressed by the following equation:

$$\begin{aligned} \hat{a}_3' &= \sqrt{T_1}\hat{a}_3 + \sqrt{1-T_1}\hat{v}_1, \quad \hat{b}_3' = \sqrt{T_2}\hat{b}_3 + \sqrt{1-T_2}\hat{v}_2, \\ \hat{a}_5 &= \sqrt{T_3}\hat{a}_4 + \sqrt{1-T_3}\hat{v}_3, \quad \hat{b}_5 = \sqrt{T_4}\hat{b}_4 + \sqrt{1-T_4}\hat{v}_4, \end{aligned} \tag{18}$$

where $\hat{v}_1$, $\hat{v}_2$, $\hat{v}_3$ and $\hat{v}_4$ are vacuum states in the input ports of the FBSs, $\hat{a}_3'$, $\hat{b}_3'$, $\hat{a}_5$ and $\hat{b}_5$ are the outputs after the FBSs. To simplify the calculation, we assume that the transmissivity on both sides is $T_e = T_3 = T_4$, which means external loss. Similarly, we assume that the internal transmissivity is $T_i = T_1 = T_2$, which means internal loss. So the slope of the intensity differ-

ence is expressed as

$$\begin{aligned}
&\frac{\partial\langle\hat{I}_{a_5}-\hat{I}_{b_5}\rangle}{\partial\phi}=\frac{\partial\langle\hat{a}_5^{\dagger}\hat{a}_5-\hat{b}_5^{\dagger}\hat{b}_5\rangle}{\partial\phi}\\
=&\frac{\partial P_{11}}{\partial\phi}(N_a\mathrm{e}^{\mathrm{i}2\theta_a})+\frac{\partial P_{12}}{\partial\phi}(1+N_a)+\frac{\partial P_{21}}{\partial\phi}N_a\\
&+\frac{\partial P_{22}}{\partial\phi}(N_a\mathrm{e}^{-\mathrm{i}2\theta_a})+\frac{\partial P_{13}}{\partial\phi}(\sqrt{N_aN_b}\,\mathrm{e}^{\mathrm{i}(\theta_a+\theta_b)})\\
&+\frac{\partial P_{14}}{\partial\phi}(\sqrt{N_aN_b}\,\mathrm{e}^{\mathrm{i}(\theta_a-\theta_b)})+\frac{\partial P_{23}}{\partial\phi}(\sqrt{N_aN_b}\,\mathrm{e}^{-\mathrm{i}(\theta_a-\theta_b)})\\
&+\frac{\partial P_{24}}{\partial\phi}\mathrm{e}^{-\mathrm{i}(\theta_a+\theta_b)})+\frac{\partial P_{31}}{\partial\phi}(\sqrt{N_aN_b}\,\mathrm{e}^{\mathrm{i}(\theta_a+\theta_b)})\\
&+\frac{\partial P_{32}}{\partial\phi}(\sqrt{N_aN_b}\,\mathrm{e}^{-\mathrm{i}(\theta_a-\theta_b)})+\frac{\partial P_{33}}{\partial\phi}(N_b\mathrm{e}^{\mathrm{i}2\theta_b})\\
&+\frac{\partial P_{34}}{\partial\phi}(1+N_b)+\frac{\partial P_{43}}{\partial\phi}N_b+\frac{\partial P_{44}}{\partial\phi}(N_b\mathrm{e}^{-\mathrm{i}2\theta_b})\\
&+\frac{\partial P_{41}}{\partial\phi}(\sqrt{N_aN_b}\,\mathrm{e}^{\mathrm{i}(\theta_a-\theta_b)})+\frac{\partial P_{42}}{\partial\phi}(\sqrt{N_aN_b}\,\mathrm{e}^{-\mathrm{i}(\theta_a+\theta_b)}),
\end{aligned}\tag{19}$$

where P_{jk} with $(j,k=1,2,3,4)$ are parameters that depend on T_i and T_e. The variance of the intensity difference can be written as

$$\begin{aligned}
\Delta^2\hat{I}=&\langle(I_{a_5}-I_{b_5})^2\rangle-\langle I_{a_5}-I_{b_5}\rangle^2\\
=&\langle\hat{a}_0\hat{a}_0\rangle L_1+\langle\hat{b}_0\hat{b}_0\rangle L_2+\langle\hat{a}_0^{\dagger}\hat{a}_0^{\dagger}\rangle L_3+\langle\hat{b}_0^{\dagger}\hat{b}_0^{\dagger}\rangle L_4\\
&+\langle\hat{b}_0\hat{a}_0^{\dagger}\rangle L_5+\langle\hat{b}_0^{\dagger}\hat{a}_0\rangle L_6+\langle\hat{b}_0\hat{a}_0\rangle L_7+\langle\hat{b}_0^{\dagger}\hat{a}_0^{\dagger}\rangle L_8\\
&+N_aL_9+N_bL_{10}+L_{11}.
\end{aligned}\tag{20}$$

In the special case where internal losses are neglected and only external losses are considered, Eq. (19) can be simplified to

$$\left|\frac{\partial}{\partial\phi}\langle\hat{I}_{-T_\mathrm{e}}\rangle\right|=T_\mathrm{e}\left|\frac{\partial}{\partial\phi}\langle\hat{I}_{-}\rangle\right|.\tag{21}$$

Similarly, by setting $T_\mathrm{i}=1$, we effectively isolate the effect of external losses, allowing Eq. (20) to be simplified to

$$\begin{aligned}
\Delta^2\hat{I}_{-T_\mathrm{e}}=&\,T_\mathrm{e}^2[(N_a+N_b)+4\sin^2\phi(\cosh^4 r-\cosh^2 r)\\
&\times(2N_a+2N_b+1)\\
&+2\sin(2\phi)\cosh r\sinh r[N_b\cos(\theta-2\theta_b)\\
&\times-N_a\cos(\theta-\theta_a)]\\
&+8\sin^2\phi\cosh r\sinh r(\cosh^2 r+\sinh^2 r)\\
&\times\sqrt{N_aN_b}\cos(\theta-\theta_a-\theta_b)]\\
&+T_\mathrm{e}(1-T_\mathrm{e})[(\cosh^2 r+\sinh^2 r)\\
&\times(N_a+N_b)+2\sinh^2 r\\
&+4\cosh r\sinh r\sqrt{N_aN_b}\cos(\theta-\theta_a-\theta_b)],
\end{aligned}\tag{22}$$

where the detailed derivations the corresponding formulae are provided in Appendix B.

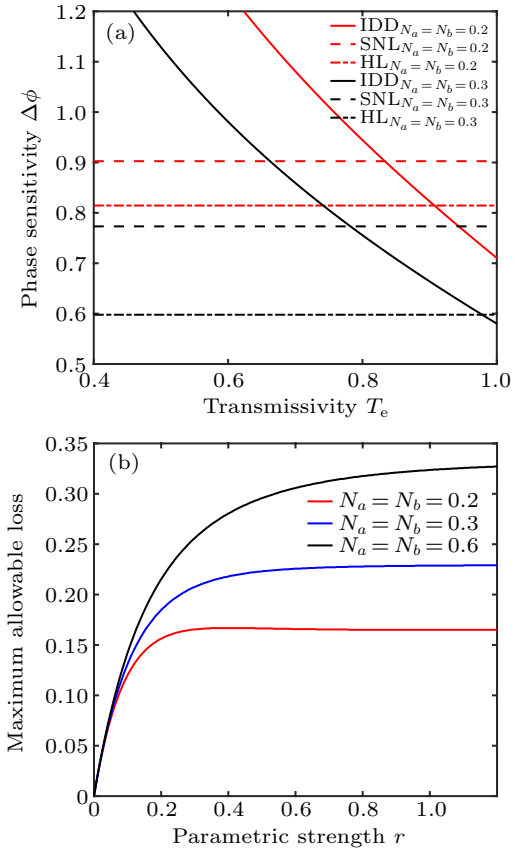


Fig. 8. (a) Phase sensitivity versus external transmissivity T_e. (b) Maximum allowable loss versus parametric strength r, photon number N_a and N_b. The red line represents $N_a=N_b=0.2$ and the black line represents $N_a=N_b=0.3$. $\theta=2\theta_a=2\theta_b=\pi/5$.

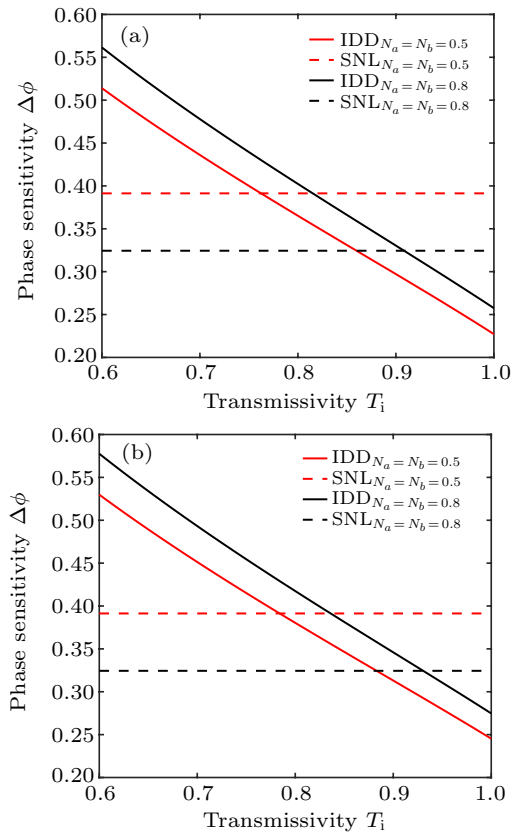


Fig. 9. (a) Phase sensitivity versus internal transmissivity T_i and (b) phase sensitivity versus both internal transmissivity T_i and external transmissivity T_e. In (b), the external loss is fixed at 0.9.

Figure 8 shows the influence of external transmissivity without internal loss on phase sensitivity. In Fig. 8(a), the red and black lines represent the cases when the photon number $N_a = N_b = 0.2$ and $N_a = N_b = 0.3$, respectively. Therefore, as the photon number increases the phase sensitivity improves. Figure 8(b) plots the maximum allowable loss versus the parametric strength r for different photon numbers. Here the maximum allowable loss is the loss below which the phase sensitivity surpasses the SNL.

Figure 9(a) illustrates the variation in phase sensitivity considering only internal losses, as well as the impact of photon number on loss tolerance. It can be observed that although an increase in photon number improves precision, it simultaneously reduces tolerance to loss. Figure 9(b) shows the effect of different photon numbers on phase sensitivity in the presence of both internal and external losses. This scenario is more experimentally relevant, as both types of losses are unavoidable in practical implementations.

4. Comparison

In this section, we compare our scheme with some existing proposals. In Ref. [49], the authors proposed a scheme which used an MZI with a single-mode squeezed vacuum state as input, and achieved a phase sensitivity below the sub-shot-noise limit. This scheme utilized dark counts and various squeezed states. By harnessing the dark counts, it surpassed the HL. In comparison, our scheme employs a two-mode squeezed coherent state and the IDD method to achieve a higher phase sensitivity. In Ref. [9], another scheme that employed an MZI with a two-mode squeezed vacuum state as input and parity detection to enhance the phase sensitivity was proposed. This scheme focused on leveraging the advantages of multiphoton catalysis rather than phase sensitivity.

Another kind of interferometer which is commonly used in precision measurement is the SU(1,1) interferometer. For example, an SU(1,1) interferometer with a thermal state input employing parity detection could surpass the SNL and approach the HL.[50] This input state is different from the squeezed states used in our scheme. Our scheme demonstrates superior performance to those interferometers. By employing a more non-classical input state, our QCRB achieves extremely high precision, providing a significant advantage in phase sensitivity. Moreover, our scheme achieves phase sensitivity surpassing the HL by using intensity difference measurement.

A similar input state was used in a modified SU(1,1) interferometer by Zhang *et al.*, as shown in Fig. 10.[41] Their approach employed two coherent states, whereas ours utilizes a two-mode squeezed coherent state. Similar to their approach, our input states are all subjected to an OPA before being fed into a linear device, which means that we have the same input mean photon number under the same input state and parametric strength. Therefore, we only need to ensure that the input photon number and parametric strength of the two schemes are the same in order to make a fair comparison. As shown in Fig. 11, we compare our scheme with the modified SU(1,1) interferometer in terms of phase sensitivity by different detection methods as well as QCRB. In Fig. 11(a) it can be observed that when $N_a = N_b = 0.5$ our scheme exhibits better phase sensitivity, with mean photon number $N = 11.48$. Additionally, as shown in Fig. 11(b), when $N_a = N_b \leq 0.96$, our scheme achieves higher precision compared with the modified SU(1,1) interferometer. Furthermore, when $N_a = N_b \leq 1$, the QCRB of our scheme also demonstrates superior phase sensitivity.

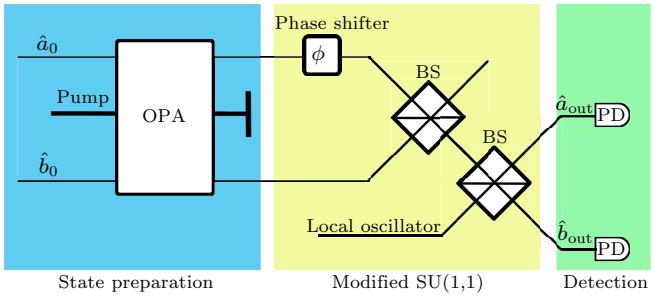


Fig. 10. Schematic of a modified SU(1,1) interferometer. OPA, optical parametric amplifier; BS, beam splitter; PD, photon detector.

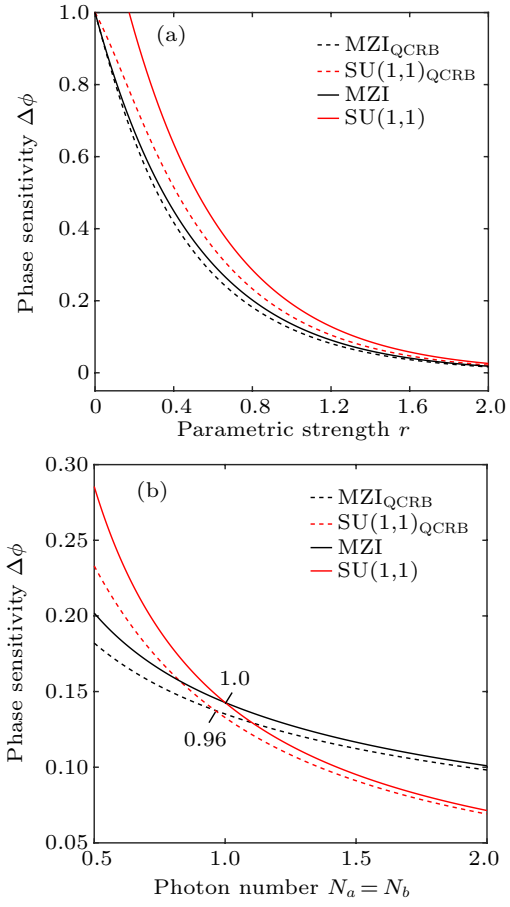


Fig. 11. (a) Phase sensitivity versus parametric strength r and (b) photon number $N_a = N_b$. $\theta = 2\theta_a = 2\theta_b = \pi/5$, $N_a = N_b = 0.5$ in (a) and $r = 0.8$ in (b).

5. Conclusion

In conclusion, a scheme based on an MZI with a two-mode squeezed coherent state input is proposed in this paper. By analyzing the impact of the parameters on phase sensitivity, we identify the points where the phase sensitivity most significantly surpasses the HL, as well as the corresponding phase-matching condition. Through optimization of the input state, we demonstrate that the phase sensitivity of our scheme with IDD can surpass the HL. We then investigate the impact of photon loss on phase sensitivity under the phase-matching condition, showing that our scheme exhibits robustness against photon loss. Moreover, it achieves higher accuracy at low photon numbers compared with existing schemes. Our work fills a gap in the study of phase sensitivity in MZIs with two-mode squeezed coherent state input and provides valuable insights for the advancement of precision measurement.

Appendix A: Derivation of the QCRB

The QCRB is given by

$$(\Delta\phi_{\mathrm{QCRB}})^2 \geq (MF(\phi))^{-1}, \tag{A1}$$

where $\Delta\phi_{\mathrm{QCRB}}$ is the variance of the parameter ϕ, $M=1$ is the number of measurements repeated and $F(\phi)$ is the quantum Fisher information, which is given by

$$F = \begin{bmatrix} F_{jj} & F_{jk} \\ F_{kj} & F_{kk} \end{bmatrix}, \tag{A2}$$

where $j,k \in (\mathrm{s},\mathrm{d})$. When the input is a pure state, the QCRB can be written as

$$\begin{aligned} &F_{jk} = 4\mathrm{Re}(\langle\partial_j\psi|\partial_k\psi\rangle - \langle\partial_j\psi|\psi\rangle\langle\psi|\partial_k\psi\rangle), \\ &\begin{bmatrix} \Delta^2\phi_{\mathrm{s}} & \Delta\phi_{\mathrm{s}}\Delta\phi_{\mathrm{d}} \\ \Delta\phi_{\mathrm{d}}\Delta\phi_{\mathrm{s}} & \Delta^2\phi_{\mathrm{d}} \end{bmatrix} \geq \frac{1}{D_F}\begin{bmatrix} F_{\mathrm{dd}} & -F_{\mathrm{sd}} \\ -F_{\mathrm{ds}} & F_{\mathrm{ss}} \end{bmatrix}, \\ &D_F = F_{\mathrm{dd}}F_{\mathrm{ss}} - F_{\mathrm{ds}}F_{\mathrm{sd}}. \end{aligned} \tag{A3}$$

Appendix B: Analysis of the influence of photon loss

In our study of internal and external losses we employ FBSs to simulate the corresponding processes. The FBSs placed before the second BS are arranged inside the interferometer to model internal losses, while those positioned after the second BS, in front of the detectors, are used to simulate detection losses, i.e. external losses. After the FBSs, the input–output relations are given by

$$\begin{aligned} \hat{a}_3' &= \sqrt{T_1}\,\hat{a}_3 + \sqrt{1-T_1}\,\hat{v}_1 \\ &= \frac{\sqrt{T_1}}{\sqrt{2}}\,\mathrm{e}^{\mathrm{i}\phi}\cosh r\,\hat{a}_0 + \mathrm{i}\frac{\sqrt{T_1}}{\sqrt{2}}\,\mathrm{e}^{\mathrm{i}\theta}\,\mathrm{e}^{\mathrm{i}\phi}\sinh r\,\hat{a}_0^\dagger \\ &\quad + \mathrm{i}\frac{\sqrt{T_1}}{\sqrt{2}}\,\mathrm{e}^{\mathrm{i}\phi}\cosh r\,\hat{b}_0 + \frac{\sqrt{T_1}}{\sqrt{2}}\,\mathrm{e}^{\mathrm{i}\theta}\,\mathrm{e}^{\mathrm{i}\phi}\sinh r\,\hat{b}_0^\dagger \\ &\quad + \sqrt{1-T_1}\,\hat{v}_1, \end{aligned} \tag{B1}$$

$$\begin{aligned} \hat{b}_3' &= \sqrt{T_2}\,\hat{b}_3 + \sqrt{1-T_2}\,\hat{v}_2 \\ &= \mathrm{i}\frac{\sqrt{T_2}}{\sqrt{2}}\cosh r\,\hat{a}_0 + \frac{\sqrt{T_2}}{\sqrt{2}}\,\mathrm{e}^{\mathrm{i}\theta}\sinh r\,\hat{a}_0^\dagger \\ &\quad + \frac{\sqrt{T_2}}{\sqrt{2}}\cosh r\,\hat{b}_0 + \mathrm{i}\frac{\sqrt{T_2}}{\sqrt{2}}\,\mathrm{e}^{\mathrm{i}\theta}\sinh r\,\hat{b}_0^\dagger \\ &\quad + \sqrt{1-T_2}\,\hat{v}_2. \end{aligned} \tag{B2}$$

The modes $\hat{a}_3'$ and $\hat{b}_3'$, after entering the second BS, are transformed into the interferometer outputs $\hat{a}_4$ and $\hat{b}_4$. These then pass through the FBSs placed before the detectors, becoming $\hat{a}_5$ and $\hat{b}_5$, and are finally detected by the PDs. After the second BS, the input–output relationship is

$$\begin{aligned} \hat{a}_4 &= \frac{1}{\sqrt{2}}\hat{a}_3' + \mathrm{i}\frac{1}{\sqrt{2}}\hat{b}_3' \\ &= \left(\frac{\sqrt{T_1}}{2}\,\mathrm{e}^{\mathrm{i}\phi}\cosh r - \frac{\sqrt{T_2}}{2}\cosh r\right)\hat{a}_0 \\ &\quad + \left(\mathrm{i}\frac{\sqrt{T_1}}{2}\,\mathrm{e}^{\mathrm{i}\theta}\,\mathrm{e}^{\mathrm{i}\phi}\sinh r + \mathrm{i}\frac{\sqrt{T_2}}{2}\,\mathrm{e}^{\mathrm{i}\theta}\sinh r\right)\hat{a}_0^\dagger \\ &\quad + \left(\mathrm{i}\frac{\sqrt{T_1}}{2}\,\mathrm{e}^{\mathrm{i}\phi}\cosh r + \frac{\sqrt{T_2}}{2}\cosh r\right)\hat{b}_0 \\ &\quad + \left(\frac{\sqrt{T_1}}{2}\,\mathrm{e}^{\mathrm{i}\theta}\,\mathrm{e}^{\mathrm{i}\phi}\sinh r - \frac{\sqrt{T_2}}{2}\,\mathrm{e}^{\mathrm{i}\theta}\sinh r\right)\hat{b}_0^\dagger \\ &\quad + \frac{\sqrt{1-T_1}}{\sqrt{2}}\hat{v}_1 + \mathrm{i}\frac{\sqrt{1-T_2}}{\sqrt{2}}\hat{v}_2, \end{aligned} \tag{B3}$$

$$\begin{aligned} \hat{b}_4 &= \mathrm{i}\frac{1}{\sqrt{2}}\hat{a}_3' + \frac{1}{\sqrt{2}}\hat{b}_3' \\ &= \left(\mathrm{i}\frac{\sqrt{T_1}}{2}\,\mathrm{e}^{\mathrm{i}\phi}\cosh r + \mathrm{i}\frac{\sqrt{T_2}}{2}\cosh r\right)\hat{a}_0 \\ &\quad + \left(-\frac{\sqrt{T_1}}{2}\,\mathrm{e}^{\mathrm{i}\theta}\,\mathrm{e}^{\mathrm{i}\phi}\sinh r + \frac{\sqrt{T_2}}{2}\,\mathrm{e}^{\mathrm{i}\theta}\sinh r\right)\hat{a}_0^\dagger \\ &\quad + \left(-\frac{\sqrt{T_1}}{2}\,\mathrm{e}^{\mathrm{i}\phi}\cosh r + \frac{\sqrt{T_2}}{2}\cosh r\right)\hat{b}_0 \\ &\quad + \left(\mathrm{i}\frac{\sqrt{T_1}}{2}\,\mathrm{e}^{\mathrm{i}\theta}\,\mathrm{e}^{\mathrm{i}\phi}\sinh r + \mathrm{i}\frac{\sqrt{T_2}}{2}\,\mathrm{e}^{\mathrm{i}\theta}\sinh r\right)\hat{b}_0^\dagger \\ &\quad + \mathrm{i}\frac{\sqrt{1-T_1}}{\sqrt{2}}\hat{v}_1 + \frac{\sqrt{1-T_2}}{\sqrt{2}}\hat{v}_2. \end{aligned} \tag{B4}$$

After passing through the second set of FBSs, which simulate external losses, $\hat{a}_5$ and $\hat{b}_5$ are received by the PDs. Thus, they undergo similar processes before detection. They can be given by

$$\begin{aligned} \hat{a}_5 &= \sqrt{T_3}\,\hat{a}_4 + \sqrt{1-T_3}\,\hat{v}_3 \\ &= M_1\hat{a}_0 + M_2\hat{a}_0^\dagger + M_3\hat{b}_0 + M_4\hat{b}_0^\dagger \\ &\quad + M_5\hat{v}_1 + M_6\hat{v}_2 + M_7\hat{v}_3, \end{aligned} \tag{B5}$$

and

$$\begin{aligned} \hat{b}_5 &= \sqrt{T_4}\,\hat{b}_4 + \sqrt{1-T_4}\,\hat{v}_4 \\ &= W_1\hat{a}_0 + W_2\hat{a}_0^\dagger + W_3\hat{b}_0 + W_4\hat{b}_0^\dagger \\ &\quad + W_5\hat{v}_1 + W_6\hat{v}_2 + W_7\hat{v}_4, \end{aligned} \tag{B6}$$

where W and M are parameters that depend on T_1, T_2, T_3, T_4, r and θ. After obtaining the output field operators, we can calculate the corresponding intensities, which are then used to determine the phase sensitivity based on IDD. The final output intensity is given by

$$\begin{aligned}
I_a = \hat{a}_5^\dagger \hat{a}_5 =& M_2^* M_1 \hat{a}_0 \hat{a}_0 + M_2^* M_2 \hat{a}_0 \hat{a}_0^\dagger + M_2^* M_3 \hat{a}_0 \hat{b}_0 + M_2^* M_4 \hat{a}_0 \hat{b}_0^\dagger + M_2^* M_5 \hat{a}_0 \hat{v}_1 + M_2^* M_6 \hat{a}_0 \hat{v}_2 + M_2^* M_7 \hat{a}_0 \hat{v}_3 \\
&+ M_1^* M_1 \hat{a}_0^\dagger \hat{a}_0 + M_1^* M_2 \hat{a}_0^\dagger \hat{a}_0^\dagger + M_1^* M_3 \hat{a}_0^\dagger \hat{b}_0 + M_1^* M_4 \hat{a}_0^\dagger \hat{b}_0^\dagger + M_1^* M_5 \hat{a}_0^\dagger \hat{v}_1 + M_1^* M_6 \hat{a}_0^\dagger \hat{v}_2 + M_1^* M_7 \hat{a}_0^\dagger \hat{v}_3 \\
&+ M_4^* M_1 \hat{b}_0 \hat{a}_0 + M_4^* M_2 \hat{b}_0 \hat{a}_0^\dagger + M_4^* M_3 \hat{b}_0 \hat{b}_0 + M_4^* M_4 \hat{b}_0 \hat{b}_0^\dagger + M_4^* M_5 \hat{b}_0 \hat{v}_1 + M_4^* M_6 \hat{b}_0 \hat{v}_2 + M_4^* M_7 \hat{b}_0 \hat{v}_3 \\
&+ M_3^* M_1 \hat{b}_0^\dagger \hat{a}_0 + M_3^* M_2 \hat{b}_0^\dagger \hat{a}_0^\dagger + M_3^* M_3 \hat{b}_0^\dagger \hat{b}_0 + M_3^* M_4 \hat{b}_0^\dagger \hat{b}_0^\dagger + M_3^* M_5 \hat{b}_0^\dagger \hat{v}_1 + M_3^* M_6 \hat{b}_0^\dagger \hat{v}_2 + M_3^* M_7 \hat{b}_0^\dagger \hat{v}_3 \\
&+ M_5 M_1 \hat{v}_1^\dagger \hat{a}_0 + M_5 M_2 \hat{v}_1^\dagger \hat{a}_0^\dagger + M_5 M_3 \hat{v}_1^\dagger \hat{b}_0 + M_5 M_4 \hat{v}_1^\dagger \hat{b}_0^\dagger + M_5 M_5 \hat{v}_1^\dagger \hat{v}_1 + M_5 M_6 \hat{v}_1^\dagger \hat{v}_2 + M_5 M_7 \hat{v}_1^\dagger \hat{v}_3 \\
&+ M_6^* M_1 \hat{v}_2^\dagger \hat{a}_0 + M_6^* M_2 \hat{v}_2^\dagger \hat{a}_0^\dagger + M_6^* M_3 \hat{v}_2^\dagger \hat{b}_0 + M_6^* M_4 \hat{v}_2^\dagger \hat{b}_0^\dagger + M_6^* M_5 \hat{v}_2^\dagger \hat{v}_1 + M_6^* M_6 \hat{v}_2^\dagger \hat{v}_2 + M_6^* M_7 \hat{v}_2^\dagger \hat{v}_3 \\
&+ M_7 M_1 \hat{v}_3^\dagger \hat{a}_0 + M_7 M_2 \hat{v}_3^\dagger \hat{a}_0^\dagger + M_7 M_3 \hat{v}_3^\dagger \hat{b}_0 + M_7 M_4 \hat{v}_3^\dagger \hat{b}_0^\dagger + M_7 M_5 \hat{v}_3^\dagger \hat{v}_1 + M_7 M_6 \hat{v}_3^\dagger \hat{v}_2 + M_7 M_7 \hat{v}_3^\dagger \hat{v}_3, \qquad \text{(B7)} \\
I_b = \hat{b}_5^\dagger \hat{b}_5 =& W_2^* W_1 \hat{a}_0 \hat{a}_0 + W_2^* W_2 \hat{a}_0 \hat{a}_0^\dagger + W_2^* W_3 \hat{a}_0 \hat{b}_0 + W_2^* W_4 \hat{a}_0 \hat{b}_0^\dagger + W_2^* W_5 \hat{a}_0 \hat{v}_1 + W_2^* W_6 \hat{a}_0 \hat{v}_2 + W_2^* W_7 \hat{a}_0 \hat{v}_4 \\
&+ W_1^* W_1 \hat{a}_0^\dagger \hat{a}_0 + W_1^* W_2 \hat{a}_0^\dagger \hat{a}_0^\dagger + W_1^* W_3 \hat{a}_0^\dagger \hat{b}_0 + W_1^* W_4 \hat{a}_0^\dagger \hat{b}_0^\dagger + W_1^* W_5 \hat{a}_0^\dagger \hat{v}_1 + W_1^* W_6 \hat{a}_0^\dagger \hat{v}_2 + W_1^* W_7 \hat{a}_0^\dagger \hat{v}_4 \\
&+ W_4^* W_1 \hat{b}_0 \hat{a}_0 + W_4^* W_2 \hat{b}_0 \hat{a}_0^\dagger + W_4^* W_3 \hat{b}_0 \hat{b}_0 + W_4^* W_4 \hat{b}_0 \hat{b}_0^\dagger + W_4^* W_5 \hat{b}_0 \hat{v}_1 + W_4^* W_6 \hat{b}_0 \hat{v}_2 + W_4^* W_7 \hat{b}_0 \hat{v}_4 \\
&+ W_3^* W_1 \hat{b}_0^\dagger \hat{a}_0 + W_3^* W_2 \hat{b}_0^\dagger \hat{a}_0^\dagger + W_3^* W_3 \hat{b}_0^\dagger \hat{b}_0 + W_3^* W_4 \hat{b}_0^\dagger \hat{b}_0^\dagger + W_3^* W_5 \hat{b}_0^\dagger \hat{v}_1 + W_3^* W_6 \hat{b}_0^\dagger \hat{v}_2 + W_3^* W_7 \hat{b}_0^\dagger \hat{v}_4 \\
&+ W_5^* W_1 \hat{v}_1^\dagger \hat{a}_0 + W_5^* W_2 \hat{v}_1^\dagger \hat{a}_0^\dagger + W_5^* W_3 \hat{v}_1^\dagger \hat{b}_0 + W_5^* W_4 \hat{v}_1^\dagger \hat{b}_0^\dagger + W_5^* W_5 \hat{v}_1^\dagger \hat{v}_1 + W_5^* W_6 \hat{v}_1^\dagger \hat{v}_2 + W_5^* W_7 \hat{v}_1^\dagger \hat{v}_4 \\
&+ W_6 W_1 \hat{v}_2^\dagger \hat{a}_0 + W_6 W_2 \hat{v}_2^\dagger \hat{a}_0^\dagger + W_6 W_3 \hat{v}_2^\dagger \hat{b}_0 + W_6 W_4 \hat{v}_2^\dagger \hat{b}_0^\dagger + W_6 W_5 \hat{v}_2^\dagger \hat{v}_1 + W_6 W_6 \hat{v}_2^\dagger \hat{v}_2 + W_6 W_7 \hat{v}_2^\dagger \hat{v}_4 \\
&+ W_7 W_1 \hat{v}_4^\dagger \hat{a}_0 + W_7 W_2 \hat{v}_4^\dagger \hat{a}_0^\dagger + W_7 W_3 \hat{v}_4^\dagger \hat{b}_0 + W_7 W_4 \hat{v}_4^\dagger \hat{b}_0^\dagger + W_7 W_5 \hat{v}_4^\dagger \hat{v}_1 + W_7 W_6 \hat{v}_4^\dagger \hat{v}_2 + W_7 W_7 \hat{v}_4^\dagger \hat{v}_4. \qquad \text{(B8)}
\end{aligned}$$

Equations (B7) and (B8) give the intensities of the two beams output from the MZI after experiencing losses. Subtracting the intensities of the two output ports yields

$$\begin{aligned}
I_a - I_b =& P_{11} \hat{a}_0 \hat{a}_0 + P_{12} \hat{a}_0 \hat{a}_0^\dagger + P_{13} \hat{a}_0 \hat{b}_0 + P_{14} \hat{a}_0 \hat{b}_0^\dagger + P_{15} \hat{a}_0 \hat{v}_1 + P_{16} \hat{a}_0 \hat{v}_2 + P_{17} \hat{a}_0 \hat{v}_3 + P_{18} \hat{a}_0 \hat{v}_4 \\
&+ P_{21} \hat{a}_0^\dagger \hat{a}_0 + P_{22} \hat{a}_0^\dagger \hat{a}_0^\dagger + P_{23} \hat{a}_0^\dagger \hat{b}_0 + P_{24} \hat{a}_0^\dagger \hat{b}_0^\dagger + P_{25} \hat{a}_0^\dagger \hat{v}_1 + P_{26} \hat{a}_0^\dagger \hat{v}_2 + P_{27} \hat{a}_0^\dagger \hat{v}_3 + P_{28} \hat{a}_0^\dagger \hat{v}_4 \\
&+ P_{31} \hat{b}_0 \hat{a}_0 + P_{32} \hat{b}_0 \hat{a}_0^\dagger + P_{33} \hat{b}_0 \hat{b}_0 + P_{34} \hat{b}_0 \hat{b}_0^\dagger + P_{35} \hat{b}_0 \hat{v}_1 + P_{36} \hat{b}_0 \hat{v}_2 + P_{37} \hat{b}_0 \hat{v}_3 + P_{38} \hat{b}_0 \hat{v}_4 \\
&+ P_{41} \hat{b}_0^\dagger \hat{a}_0 + P_{42} \hat{b}_0^\dagger \hat{a}_0^\dagger + P_{43} \hat{b}_0^\dagger \hat{b}_0 + P_{44} \hat{b}_0^\dagger \hat{b}_0^\dagger + P_{45} \hat{b}_0^\dagger \hat{v}_1 + P_{46} \hat{b}_0^\dagger \hat{v}_2 + P_{47} \hat{b}_0^\dagger \hat{v}_3 + P_{48} \hat{b}_0^\dagger \hat{v}_4 \\
&+ P_{51} \hat{v}_1^\dagger \hat{a}_0 + P_{52} \hat{v}_1^\dagger \hat{a}_0^\dagger + P_{53} \hat{v}_1^\dagger \hat{b}_0 + P_{54} \hat{v}_1^\dagger \hat{b}_0^\dagger + P_{55} \hat{v}_1^\dagger \hat{v}_1 + P_{56} \hat{v}_1^\dagger \hat{v}_2 + P_{57} \hat{v}_1^\dagger \hat{v}_3 + P_{58} \hat{v}_1^\dagger \hat{v}_4 \\
&+ P_{61} \hat{v}_2^\dagger \hat{a}_0 + P_{62} \hat{v}_2^\dagger \hat{a}_0^\dagger + P_{63} \hat{v}_2^\dagger \hat{b}_0 + P_{64} \hat{v}_2^\dagger \hat{b}_0^\dagger + P_{65} \hat{v}_2^\dagger \hat{v}_1 + P_{66} \hat{v}_2^\dagger \hat{v}_2 + P_{67} \hat{v}_2^\dagger \hat{v}_3 + P_{68} \hat{v}_2^\dagger \hat{v}_4 \\
&+ P_{71} \hat{v}_3^\dagger \hat{a}_0 + P_{72} \hat{v}_3^\dagger \hat{a}_0^\dagger + P_{73} \hat{v}_3^\dagger \hat{b}_0 + P_{74} \hat{v}_3^\dagger \hat{b}_0^\dagger + P_{75} \hat{v}_3^\dagger \hat{v}_1 + P_{76} \hat{v}_3^\dagger \hat{v}_2 + P_{77} \hat{v}_3^\dagger \hat{v}_3 \\
&+ P_{81} \hat{v}_4^\dagger \hat{a}_0 + P_{82} \hat{v}_4^\dagger \hat{a}_0^\dagger + P_{83} \hat{v}_4^\dagger \hat{b}_0 + P_{84} \hat{v}_4^\dagger \hat{b}_0^\dagger + P_{85} \hat{v}_4^\dagger \hat{v}_1 + P_{86} \hat{v}_4^\dagger \hat{v}_2 + P_{87} \hat{v}_4^\dagger \hat{v}_4. \qquad \text{(B9)}
\end{aligned}$$

By subtracting the two output intensities and applying the IDD formula we obtain the corresponding phase sensitivity, which consists of two parts: the variance of the intensity difference and the slope of the intensity difference. So the variance of the intensity difference can be written as

$$\begin{aligned}
&\Delta^2 \hat{I} = \langle (I_a - I_b)^2 \rangle - \langle I_a - I_b \rangle^2 \\
=& \langle \hat{a}_0 \hat{a}_0 \rangle L_1 + \langle \hat{b}_0 \hat{b}_0 \rangle L_2 + \langle \hat{a}_0^\dagger \hat{a}_0^\dagger \rangle L_3 + \langle \hat{b}_0^\dagger \hat{b}_0^\dagger \rangle L_4 + \langle \hat{b}_0 \hat{a}_0^\dagger \rangle L_5 + \langle \hat{b}_0^\dagger \hat{a}_0 \rangle L_6 + \langle \hat{b}_0 \hat{a}_0 \rangle L_7 + \langle \hat{b}_0^\dagger \hat{a}_0^\dagger \rangle L_8 + N_a L_9 + N_b L_{10} + L_{11}, \qquad \text{(B10)}
\end{aligned}$$

and the slope of the intensity difference is expressed as

$$\begin{aligned}
&\frac{\partial \langle \hat{I}_{a_5} - \hat{I}_{b_5} \rangle}{\partial \phi} = \frac{\partial \langle \hat{a}_5^\dagger \hat{a}_5 - \hat{b}_5^\dagger \hat{b}_5 \rangle}{\partial \phi} \\
=& \frac{\partial P_{11}}{\partial \phi} (N_a \mathrm{e}^{\mathrm{i}2\theta_a}) + \frac{\partial P_{12}}{\partial \phi} (1 + N_a) + \frac{\partial P_{21}}{\partial \phi} N_a + \frac{\partial P_{22}}{\partial \phi} (N_a \mathrm{e}^{-\mathrm{i}2\theta_a}) + \frac{\partial P_{13}}{\partial \phi} (\sqrt{N_a N_b} \mathrm{e}^{\mathrm{i}(\theta_a + \theta_b)}) + \frac{\partial P_{14}}{\partial \phi} (\sqrt{N_a N_b} \mathrm{e}^{\mathrm{i}(\theta_a - \theta_b)}) \\
&+ \frac{\partial P_{23}}{\partial \phi} (\sqrt{N_a N_b} \mathrm{e}^{-\mathrm{i}(\theta_a - \theta_b)}) + \frac{\partial P_{24}}{\partial \phi} \mathrm{e}^{-\mathrm{i}(\theta_a + \theta_b)}) + \frac{\partial P_{31}}{\partial \phi} (\sqrt{N_a N_b} \mathrm{e}^{\mathrm{i}(\theta_a + \theta_b)}) + \frac{\partial P_{32}}{\partial \phi} (\sqrt{N_a N_b} \mathrm{e}^{-\mathrm{i}(\theta_a - \theta_b)}) \\
&+ \frac{\partial P_{33}}{\partial \phi} (N_b \mathrm{e}^{\mathrm{i}2\theta_b}) + \frac{\partial P_{34}}{\partial \phi} (1 + N_b) + \frac{\partial P_{43}}{\partial \phi} N_b + \frac{\partial P_{44}}{\partial \phi} (N_b \mathrm{e}^{-\mathrm{i}2\theta_b}) + \frac{\partial P_{41}}{\partial \phi} (\sqrt{N_a N_b} \mathrm{e}^{\mathrm{i}(\theta_a - \theta_b)}) + \frac{\partial P_{42}}{\partial \phi} (\sqrt{N_a N_b} \mathrm{e}^{-\mathrm{i}(\theta_a + \theta_b)}), \qquad \text{(B11)}
\end{aligned}$$

where L_i $(i = 1,2,3,4,5,6,7,8,9,10,11)$ are parameters that depend on P_{jk}. The explicit expressions for L_i are given by

$$
\begin{aligned}
L_1 &= \left(2P_{11}P_{12} + 2P_{11}P_{21} + P_{13}P_{14} + P_{15}P_{51} + P_{17}P_{71} + P_{31}P_{14} + P_{31}P_{41} + P_{16}P_{61} + P_{18}P_{81} + P_{13}P_{41}\right),\\
L_2 &= \left(P_{13}P_{23} + P_{13}P_{32} + P_{31}P_{23} + P_{31}P_{32} + 2P_{33}P_{34} + 2P_{33}P_{43} + P_{35}P_{53} + P_{36}P_{63} + P_{37}P_{73} + P_{38}P_{83}\right),\\
L_3 &= \left(2P_{12}P_{22} + 2P_{21}P_{22} + P_{23}P_{42} + P_{23}P_{24} + P_{32}P_{42} + P_{32}P_{24} + P_{25}P_{52} + P_{26}P_{62} + P_{27}P_{72} + P_{28}P_{82}\right),\\
L_4 &= \left(P_{14}P_{24} + P_{14}P_{42} + 2P_{34}P_{44} + P_{41}P_{24} + P_{41}P_{42} + 2P_{43}P_{44} + P_{47}P_{74} + P_{45}P_{54} + P_{46}P_{64} + P_{48}P_{84}\right),\\
L_5 &= \left(P_{12}P_{32} + P_{21}P_{32} + 2P_{31}P_{22} + P_{32}P_{34} + P_{32}P_{43} + 2P_{33}P_{24} + 2P_{33}P_{42} + P_{35}P_{52} + P_{36}P_{62} + P_{37}P_{72}\right.\\
&\quad \left. + P_{38}P_{82} + P_{12}P_{23} + 2P_{13}P_{22} + P_{21}P_{23} + P_{23}P_{34} + P_{23}P_{43} + P_{25}P_{53} + P_{26}P_{63} + P_{27}P_{73} + P_{28}P_{83}\right),\\
L_6 &= \left(P_{34}P_{41} + P_{41}P_{12} + P_{41}P_{21} + P_{43}P_{41} + P_{45}P_{51} + P_{46}P_{61} + P_{47}P_{71} + P_{48}P_{81} + 2P_{11}P_{24} + 2P_{11}P_{42}\right.\\
&\quad \left. + 2P_{13}P_{44} + P_{14}P_{12} + P_{14}P_{21} + P_{15}P_{54} + P_{18}P_{84} + P_{34}P_{14} + P_{16}P_{64} + P_{17}P_{74} + P_{43}P_{14} + 2P_{31}P_{44}\right),\\
L_7 &= \left(P_{31}P_{12} + P_{31}P_{21} + P_{31}P_{34} + P_{31}P_{43} + 2P_{33}P_{14} + 2P_{33}P_{41} + P_{35}P_{51} + P_{36}P_{61} + P_{37}P_{71} + P_{38}P_{81}\right.\\
&\quad \left. + 2P_{11}P_{23} + 2P_{11}P_{32} + P_{13}P_{12} + P_{13}P_{21} + P_{13}P_{34} + P_{13}P_{43} + P_{15}P_{53} + P_{16}P_{63} + P_{17}P_{73} + P_{18}P_{83}\right),\\
L_8 &= \left(P_{12}P_{42} + P_{21}P_{42} + P_{34}P_{42} + 2P_{41}P_{22} + P_{43}P_{42} + P_{45}P_{52} + P_{46}P_{62} + P_{47}P_{72} + P_{48}P_{82} + P_{12}P_{24}\right.\\
&\quad \left. + 2P_{14}P_{22} + P_{21}P_{24} + 2P_{23}P_{44} + 2P_{32}P_{44} + P_{34}P_{24} + P_{43}P_{24} + P_{25}P_{54} + P_{27}P_{74} + P_{26}P_{64} + P_{28}P_{84}\right),\\
L_9 &= \left(P_{12}P_{12} + P_{12}P_{21} + P_{21}P_{12} + P_{21}P_{21} + P_{23}P_{14} + P_{23}P_{41} + P_{32}P_{14} + P_{32}P_{41} + P_{25}P_{51} + P_{26}P_{61} + P_{27}P_{71}\right.\\
&\quad \left. + P_{28}P_{81} + 4P_{11}P_{22} + P_{13}P_{42} + P_{13}P_{24} + P_{31}P_{24} + P_{31}P_{42} + P_{15}P_{52} + P_{16}P_{62} + P_{17}P_{72} + P_{18}P_{82}\right),\\
L_{10} &= \left(P_{14}P_{23} + P_{14}P_{32} + P_{41}P_{23} + P_{41}P_{32} + P_{43}P_{34} + P_{43}P_{43} + P_{45}P_{53} + P_{48}P_{83} + P_{46}P_{63} + P_{47}P_{73} + P_{34}P_{34}\right.\\
&\quad \left. + P_{34}P_{43} + P_{13}P_{42} + P_{13}P_{24} + 4P_{33}P_{44} + P_{31}P_{24} + P_{31}P_{42} + P_{35}P_{54} + P_{36}P_{64} + P_{37}P_{74} + P_{38}P_{84}\right),\\
L_{11} &= +2P_{11}P_{22} + P_{13}P_{42} + P_{13}P_{24} + 2P_{33}P_{44} + P_{31}P_{24} + P_{31}P_{42}\\
&\quad + P_{15}P_{52} + P_{16}P_{62} + P_{17}P_{72} + P_{18}P_{82} + P_{35}P_{54} + P_{36}P_{64} + P_{37}P_{74} + P_{38}P_{84}.
\end{aligned}
$$

Acknowledgements

This work was supported by the National Natural Science Foundation of China (Grant Nos. 12104190, 12104189, 12204312), the Natural Science Foundation of Jiangsu Province (Grant No. BK20210874), General project of Natural Science Research in Colleges And Universities of Jiangsu Province (Grant No. 20KJB140008), the Jiangxi Provincial Natural Science Foundation (Grant Nos. 20224BAB211014 and 20232BAB201042), and Key Laboratory of TianQin Project (Sun Yat-sen University).

References

[1] Rarity J G, Tapster P R, Jakeman E, Larchuk T, Campos R A, Teich M C and Saleh B E A 1990 *Phys. Rev. Lett.* **65** 1348

[2] Luo W, Wu C, Du Y, Zhao C, Yu M, Zhu P, Zhang K and Xu P 2024 *Chin. Phys. B* **33** 100305

[3] Wu D, Li X, Wang L L, Zhang J S, Chen W, Wang Y, Wang H J, Li J G, Yin X J, Wu Y D, An J M and Song Z G 2023 *Chin. Phys. B* **32** 010305

[4] Hudelist F, Kong J, Liu C, Jing J, Ou Z and Zhang W 2014 *Nat. Commun.* **5** 3049

[5] Nagata T, Okamoto R, O'Brien J L, Sasaki K and Takeuchi S 2007 *Science* **316** 726

[6] Kacprowicz M, Demkowicz-Dobrzański R, Wasilewski W, Banaszek K and Walmsley I 2010 *Nat. Photon.* **4** 357

[7] Goda K, Miyakawa O, Mikhailov E E, Saraf S, Adhikari R, McKenzie K, Ward R, Vass S, Weinstein A J and Mavalvala N 2008 *Nat. Phys.* **4** 472

[8] Genoni M G, Olivares S, Brivio D, Cialdi S, Cipriani D, Santamato A, Vezzoli S and Paris M G 2012 *Phys. Rev. A* **85** 043817

[9] Zhang H, Ye W, Wei C, Xia Y, Chang S, Liao Z and Hu L 2021 *Phys. Rev. A* **103** 013705

[10] Zuo X, Yan Z, Feng Y, Ma J, Jia X, Xie C and Peng K 2020 *Phys. Rev. Lett.* **124** 173602

[11] Liu J, Wang Y, Zhang M, Wang J, Wei D and Gao H 2020 *Opt. Express* **28** 39443

[12] Anisimov P M, Raterman G M, Chiruvelli A, Plick W N, Huver S D, Lee H and Dowling J P 2010 *Phys. Rev. Lett.* **104** 103602

[13] Liu P, Wang P, Yang W, Jin G and Sun C 2017 *Phys. Rev. A* **95** 023824

[14] Boto A N, Kok P, Abrams D S, Braunstein S L, Williams C P and Dowling J P 2000 *Phys. Rev. Lett.* **85** 2733

[15] Dowling J P 2008 *Contemporary Physics* **49** 125

[16] Liu J, Liu W, Li S, Wei D, Gao H and Li F 2017 *Photon. Res.* **5** 617

[17] Wang G, Li Z, Qin X, Yang Z, Li X, Wu X, Zhou Y and Chen Y 2024 *Optics & Laser Technology* **176** 110984

[18] Giovannetti V, Lloyd S and Maccone L 2011 *Nat. Photon.* **5** 222

[19] Ge W, Jacobs K, Eldredge Z, Gorshkov A V and Foss-Feig M 2018 *Phys. Rev. Lett.* **121** 043604

[20] Seshadreesan K P, Anisimov P M, Lee H and Dowling J P 2011 *New J. Phys.* **13** 083026

[21] Caves C M 1981 *Phys. Rev. D* **23** 1693

[22] Ou Z 1996 *Phys. Rev. Lett.* **77** 2352

[23] Haldar S, Barge P J, Xiao X Q and Lee H 2023 *AVS Quantum Science* **5** 034401

[24] Xiao M, Wu L A and Kimble H J 1987 *Phys. Rev. Lett.* **59** 278

[25] Grangier P, Roger G and Aspect A 1986 *Europhys. Lett.* **1** 173

[26] Giovannetti V, Lloyd S and Maccone L 2004 *Science* **306** 1330

[27] Berry D W, Higgins B L, Bartlett S D, Mitchell M W, Pryde G J and Wiseman H M 2009 *Phys. Rev. A* **80** 052114

[28] Ben-Aryeh Y 2012 *J. Opt. Soc. Am. B* **29** 2754

[29] Hall M J, Berry D W, Zwierz M and Wiseman H M 2012 *Phys. Rev. A* **85** 041802

[30] Zhang J D, Li C, Hou L and Wang S 2025 *Chin. Phys. B* **34** 010304

[31] Li D, Yuan C H, Ou Z and Zhang W 2014 *New J. Phys.* **16** 073020

[32] Liu J, Shao T, Wang Y, Zhang M, Hu Y, Chen D and Wei D 2023 *Opt. Express* **31** 27735
[33] Liu J, Shao T, Li C, Zhang M, Hu Y, Chen D and Wei D 2024 *Chin. Phys. B* **33** 014203
[34] Wang Y, Li S, Hu Y, Zhang M and Liu J 2022 *Journal of Physics Communications* **6** 035004
[35] Braunstein S L and Caves C M 1994 *Phys. Rev. Lett.* **72** 3439
[36] Yu J, Qin Y, Qin J, Wang H, Yan Z, Jia X and Peng K 2020 *Phys. Rev. Appl.* **13** 024037
[37] Ataman S, Preda A and Ionicioiu R 2018 *Phys. Rev. A* **98** 043856
[38] Liu J, Yu Y, Wang C, Chen Y, Wang J, Chen H, Wei D, Gao H and Li F 2020 *New J. Phys.* **22** 013031
[39] Zhang H, Ye W, Wei C, Liu C, Liao Z and Hu L 2021 *Phys. Rev. A* **103** 052602
[40] Liu S, Lou Y and Jing J 2019 *Phys. Rev. Lett.* **123** 113602
[41] Zhang J D, You C, Li C and Wang S 2021 *Phys. Rev. A* **103** 032617
[42] Ou Z 2012 *Phys. Rev. A* **85** 023815
[43] Lang M D and Caves C M 2013 *Phys. Rev. Lett.* **111** 173601
[44] Sparaciari C, Olivares S and Paris M G A 2016 *Phys. Rev. A* **93** 023810
[45] Gong Q K, Li D, Yuan C H, Qu Z Y and Zhang W P 2017 *Chin. Phys. B* **26** 094205
[46] Jarzyna M and Demkowicz-Dobrzański R 2012 *Phys. Rev. A* **85** 011801
[47] Takeoka M, Seshadreesan K P, You C, Izumi S and Dowling J P 2017 *Phys. Rev. A* **96** 052118
[48] Preda A and Ataman S 2019 *Phys. Rev. A* **99** 053810
[49] Zhang J D, You C and Wang S 2022 *Opt. Express* **30** 43143
[50] Ma X, You C, Adhikari S, Matekole E S, Glasser R T, Lee H and Dowling J P 2018 *Opt. Express* **26** 18492